PROCEEDINGS OF SPIE

SPIEDigitalLibrary.org/conference-proceedings-of-spie

Visualizing nanoscale spin waves using MAXYMUS

Joachim Gräfe, Markus Weigand M.D., Bartel Van Waeyenberge, Ajay Gangwar, Felix Groß, et al.

Joachim Gräfe, Markus Weigand M.D., Bartel Van Waeyenberge, Ajay Gangwar, Felix Groß, Filip Lisiecki, Justyna Rychly, Hermann Stoll, Nick Träger, Johannes Förster, Feliks Stobiecki, Janusz Dubowik, Jaroslaw Klos, Maciej Krawczyk, Christian H. Back, Eberhard J. Goering, Gisela Schütz, "Visualizing nanoscale spin waves using MAXYMUS," Proc. SPIE 11090, Spintronics XII, 1109025 (16 September 2019); doi: 10.1117/12.2530326

SPIE.

Event: SPIE Nanoscience + Engineering, 2019, San Diego, California, United States

Visualizing nanoscale spin waves using MAXYMUS

Joachim Gräfe[a], Markus Weigand[a,b], Bartel Van Waeyenberge[c], Ajay Gangwar[e], Felix Groß[a], Filip Lisiecki[g], Justyna Rychly[h], Hermann Stoll[a,d], Nick Träger[a], Johannes Förster[a], Feliks Stobiecki[g], Janusz Dubowik[g], Jaroslaw Klos[h], Maciej Krwaczyk[h], Christian H. Back[e,f], Eberhard J. Goering[a], and Gisela Schütz[a]

[a]Max Planck Institute for Intelligent Systems, Heisenbergstraße 3, 70569 Stuttgart, Germany
[b]Helmholtz-Zentrum Berlin, Albert-Einstein-Straße 15, 12489 Berlin, Germany
[c]Universiteit Gent, Krijgslaan 281, 9000 Gent, Belgium
[d]Johannes Gutenberg University, Staudingerweg 7, 55128 Mainz, Germany
[e]University of Regensburg, Universitätstraße 31, 93053 Regensburg, Germany
[f]Technical University of Munich, James-Franck-Straße 1, 85748 Garching, Germany
[g]Institute of Molecular Physics, Poznan, Poland
[h]Adam Mickiewicz University, Poznan, Poland

ABSTRACT

Magnonics research, *i.e.* the manipulation of spin waves for information processing, is a topic of intense research interest in the past years. FMR, BLS and MOKE measurements lead to tremendous success and advancement of the field. However, these methods are limited in their spatial resolution. X-ray microscopy opens up a way to push to spatial resolutions below 100 nm. Here, we discuss the methodology of STXM for pump-probe data acquisition with single photon counting and arbitrary excitation patterns. Furthermore, we showcase these capabilities using two magnonic crystals as examples: an antidot lattice and a Fibonacci quasicrystal.

Keywords: X-Ray Microscopy, X-Ray Circular Magnetic Dichrosim, Magnonics, Spin Waves, Spintronics, Spin Currents

1. INTRODUCTION

Manipulation of spin waves, the so called field of magnonics, has gained significant scientific interest in the past years.[1–4] For that purpose nano-structured materials with locally alternating magnetic properties are utilized. By structuring on the length scale of the exchange and dipole interactions, the dispersion properties of spin waves can be engineered.[2–4] These nanostructures have great potential for technological applications in data processing and storage, as well as spintronics.[3,4] However, the spin wave behaviour is not only altered on the nano-scale, but it can be directly imaged by advanced x-ray microscopy with magnetic contrast (MAXYMUS@BESSY II) with a spatial and temporal resolution of 18 nm and 35 ps respectively. Thus, emergent spin wave phenomena can be directly observed in real space on a scale beyond the capabilities of conventional BLS or MOKE measurements.

In the first part of the paper, we will present new techniques for time-resolved x-ray microscopy including ultra-sensitive detection of spin deflection angles[5] and arbitrary excitation signal generation. In the second part, we will showcase these capabilities for two examples of magnonic crystals: a regular magnonic crystal based on antidots; and propagation, extinction and localization of spin waves in a magnonic quasicrystal.[6,7]

2. METHODOLOGY

While there are several powerful x-ray microscopy techniques like photo emission electron microscopy and full-field transmission x-ray microscopy that are capable of nanoscale magnetic imaging,[8] here, we focus on scanning transmission x-ray microscopy (STXM). The fundamental operation principle of this technique is sketched in

Further author information: (Send correspondence to J.G.)
J.G.: E-mail: graefe@is.mpg.de, Telephone: +49-711-689-1852

Spintronics XII, edited by Henri-Jean M. Drouhin, Jean-Eric Wegrowe, Manijeh Razeghi, Henri Jaffrès,
Proc. of SPIE Vol. 11090, 1109025 · © 2019 SPIE · CCC code: 0277-786X/19/$21 · doi: 10.1117/12.2530326

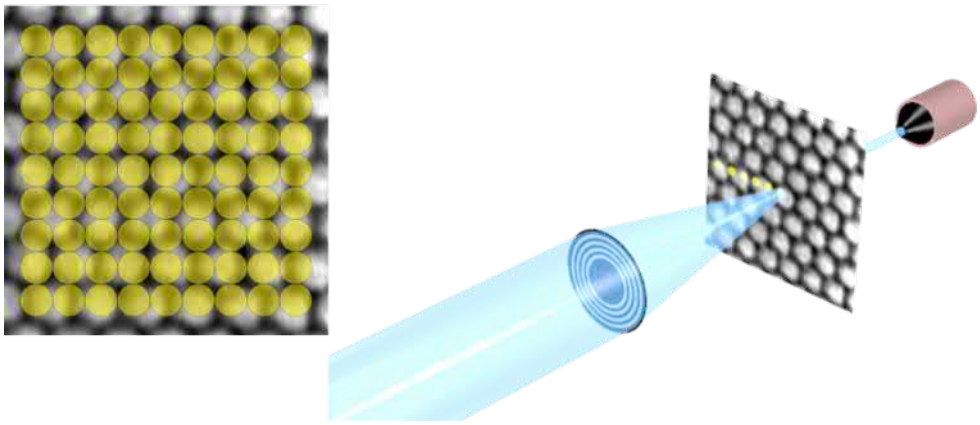

Figure 1: Simplified schematic of the STXM operation principle: an x-ray beam is focused using a Fresnel zone plate. The transmitted intensity is measured by a point detector. The image is formed by scanning the sample across the x-ray focus spot. The individual measurement positions, that are captured by the focused x-ray beam, are indicated by yellow circles.

Fig. 1. In STXM the x-ray beam is focused by a Fresnel zone plate. The sample is scanned across this x-ray focal spot to form an image. As only a single spot of the sample is illuminated, the detectors used for signal acquisition do not need to be spatially resolving and multiple detectors can be used simultaneously.[9] X-ray magnetic circular dichroism (XMCD) can easily be used for magnetization contrast.[10]

2.1 Time Interleaved Detection

For time resolved measurements, the inherent stroboscopic nature of synchrotron sources is leveraged to realize pump-probe experiments.[11] For a simple time resolved measurement, the pump can be synchronized to the synchrotron bunch clock f_{bunch}, *i.e.* 500 MHz in the case of BESSY II. If the pump excitation frequency f_{pump} is an integer multiple M of the synchrotron bunch clock

$$f_{\mathrm{pump}} = f_{\mathrm{bunch}} \cdot M, \tag{1}$$

the x-ray flashes always probe the same phase of the excitation signal. This is illustrated in Fig. 2a. In this synchronous scheme, a full image is acquired for a given phase and subsequently the phase of the pump signal is shifted with respect to the synchrotron bunch clock. This scheme does not require a fast detector, however, the accessible excitation frequencies are limited and the subsequent acquisition of the individual time frames is prone to drift artifacts.

Advancing towards more sophisticated measurement schemes requires the discrimination and individual detection of the x-ray flashes from the synchrotron source, that arrive every 2 ns in the case of BESSY II. This is achieved by using an avalanche photo diode (APD)[11,12] that recovers faster, *i.e.* in less than 1.5 ns.[11] With this fast detector single photon counting becomes possible. Therefor the APD signal is only acquired in a short detection window, *e.g.* 20 ps, that coincides with the expected arrival time of the photons,[11] thereby realizing a lock-in detection scheme for the transmitted x-ray probe. On a hardware level, this is achieved by using a fast emitter coupled logic (ECL) flip-flop to compare the APD signal to a threshold value.

Leveraging this excitation scheme, the sample's response can be probed every 2 ns and sub-harmonics of f_{bunch} can be probed with:

$$f_{\mathrm{pump}} = \frac{f_{\mathrm{bunch}}}{N}, \tag{2}$$

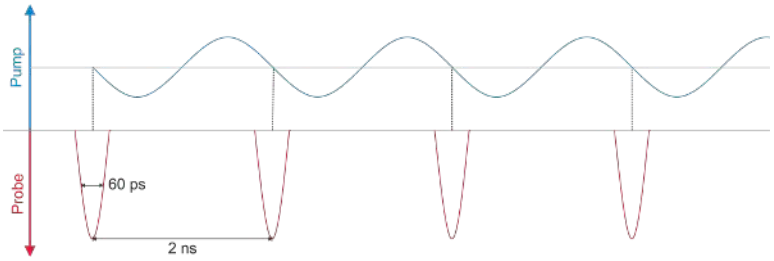

(a) Synchronous excitation with harmonics M of the synchrotron bunch clock. In this schematic example M equals 1. Each x-ray pulses probe the same phase of the pump excitation.

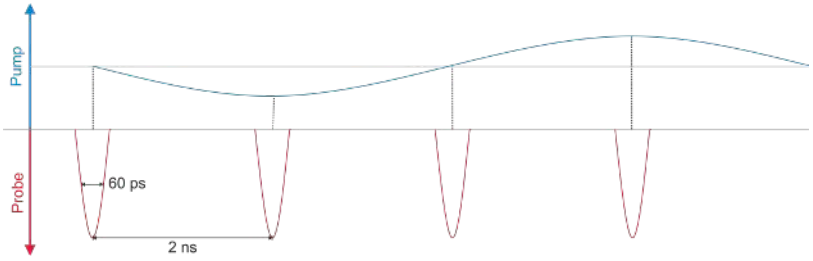

(b) Synchronous excitation with sub-harmonics N of the synchrotron bunch clock. In this schematic example N equals 5. Subsequent x-ray pulses probe consecutive phases of the pump excitation.

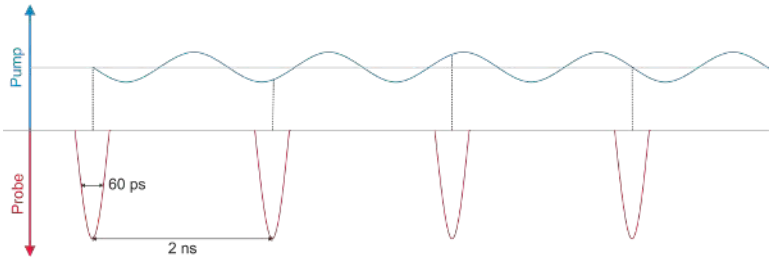

(c) Asynchronous excitation with $\frac{M}{N}$ frequency. In this schematic example M equals 4 and N equals 3. Subsequent x-ray pulses probe interleaving phases of the pump excitation.

Figure 2: Pump-probe excitation schemes used for time resolved x-ray microscopy.

where N is the number of phases of the excitation that are probed, which is illustrated in Fig. 2b. Every N-th x-ray flash probes the same phase of the exciation pump.[11] To acquire meaningful data, the individual photon signals need to be sorted consecutively according to their phase with respect to the excitation pump. This is typically achieved wtih field-programmable gate array (FPGA) hardware.[11,12] Acquiring all N time frames quasi-simultaneously will significantly reduce drift as discussed above and represents a lock-in detection of the pump signal.

While the two previously discussed acquisition schemes are limited to harmonics ($f_{\mathrm{bunch}} \cdot M$) and sub-harmonics ($\frac{f_{\mathrm{bunch}}}{N}$) of the synchrotron bunch clock, it is desirable to detect arbitrary frequencies. This can be achieved by asynchronous excitation at

$$f_{\mathrm{pump}} = f_{\mathrm{bunch}} \cdot \frac{M}{N}, \tag{3}$$

which is illustrated in Fig. 2c. Here, the excitation period is again sampled in N time frames, but the x-ray flashes do not illuminate them consecutively and the subsequently acquired time frames need to be sorted accordingly. Operating at a fractional multiple ensures that synchronization with the synchrotron is regained after N excitation periods while allowing for almost arbitrary frequencies to be used as pump.[11] The proper

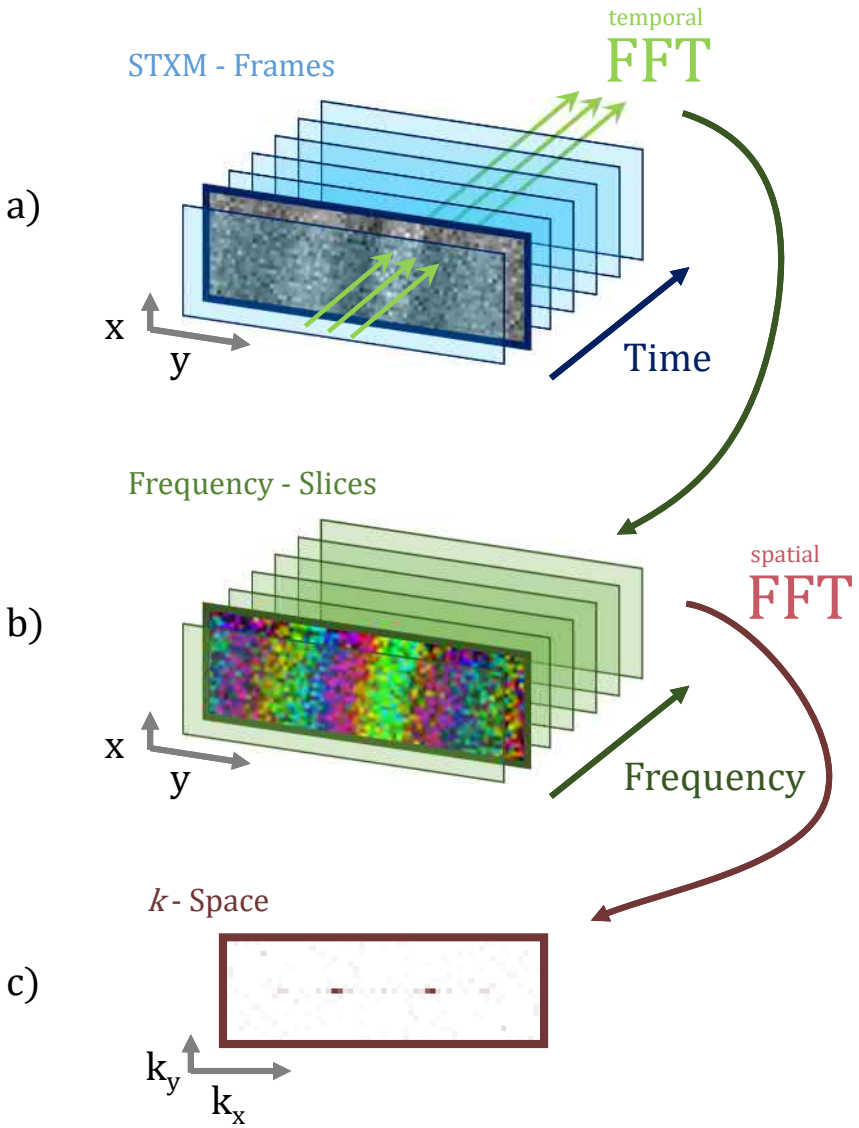

Figure 3: Schematic of the data analysis scheme: *(a)* raw temporal and spatially resolved magnetization $M(x, y, t)$ data. *(b)* spatially resolved phase $\Phi(x, y, f)$ (colour) and amplitude $A(x, y, f)$ (brightness) in the frequency domain recovered by a pixel-wise FFT. *(c)* k-vectors $\mathcal{K}(k_x, k_y, f)$ revealed by spatial FFT. Reproduced from.[5]

index position i_{sort} of an individual frame in the sequence i_{raw} is given by:

$$i_{\text{sort}} = i_{\text{raw}} \cdot M \pmod{N} \tag{4}$$

2.2 Data Analysis

The raw data acquired in a STXM measurement represents the spatially and temporal resolved x-ray absorption $\mu(x, y, t)$ that is normalized to the time averaged absorption to yield the dynamic magnetization $M(x, y, t)$. In the example data shown in Fig. 3a, a spin wave is already visible in this unprocessed gray scale image. Additional information can be gained by a pixel-wise fast Fourier transformation (FFT) in time. The FFT yields the spatially resolved phase $\Phi(x, y, f)$ and amplitude $A(x, y, f)$ in the frequency domain. Fig 3b illustrates

this, encoding amplitude A in brightness and phase Φ in colour. This allows the separation of different spin wave modes in the system. Further processing by a spatial FFT transforms the data into k-space and yields $\mathcal{K}(k_x, k_y, f)$ which gives access to the k-vectors of the spin waves excited at each frequency.[5]

Additionally, the data can be normalized to XMCD reference spectra to access absolute values for the dynamic magnetization deflection, *i.e.* the out-of-plane magnetization component and, thus, the cone angle of spin oscillations. The XMCD contrast is given by the scalar product $M \cdot \sigma$ and depends both on the magnetization M and the helicity σ of the x-rays. The XMCD magnitude can be calculated from the x-ray absorption spectra (XAS) with parallel ($\uparrow\uparrow$) and anti-parallel ($\uparrow\downarrow$) orientations of M and σ, and normalizing it in the same way as the dynamic magnetization data:

$$\mathrm{XMCD} = 2 \cdot \frac{\mathrm{XAS}_{\uparrow\uparrow} - \mathrm{XAS}_{\uparrow\downarrow}}{\mathrm{XAS}_{\uparrow\uparrow} + \mathrm{XAS}_{\uparrow\downarrow}}. \tag{5}$$

Subsequently, the normalized XMCD contrast allows for calculation of the absolute spin deflection angle Θ from the spin wave amplitude data $A(x, y, f)$:[5]

$$\Theta = \arcsin\left(\frac{A(x, y, f)}{\mathrm{XMCD}}\right). \tag{6}$$

2.3 Arbitrary Waveform Generation

The generation of simple continous wave (CW) radio frequency (RF) excitations is straight forward using fractional $\frac{M}{N}$ multipliers synchronized to the bunch clock f_{bunch}. However, more complex patterns like RF bursts, ultra-short pulses or multi-tone excitations are desirable for contemporary experiments. This can be achieved with modern arbitrary waveform generators (AWG). Here, we use a Keysight M8195A operating at 64 GSa/s. The same requirements for the asynchronous CW excitation are also valid for more complex patterns, *i.e.* the pattern consisting of samples S needs to repeat M times while N time steps are acquired ($2\,\mathrm{ns} \cdot N$). Thus, the sampling rate f_{sample} of the AWG needs to be adjusted to allow an integer number of samples in this time:

$$f_{\mathrm{sample}} = \frac{P}{F} \cdot \frac{f_{\mathrm{Bunch}}}{N}, \tag{7}$$

where P and F are integers depending on the internal clocking requirements and the precision of the prescaler P and the fractional divider F of the AWG. Any mismatch between the sampling frequency f_{sample} and the synchrotron reference $S \cdot \frac{M}{N} \cdot f_{\mathrm{Bunch}}$ will result in excitation pump jitter and degrade time resolution. While the initial synchronization is cumbersome, the use of an AWG opens up a vast range of excitation patterns to x-ray microscopic detection. Combining a multi-tone excitation, *e.g.* a sinc pulse, with the frequency and k-vector analysis discussed above, yields a vast amount of information from a single measurement.

3. RESULTS

In the following the capabilities of STXM for magnonics research are showcased. Therefor two types of magnonic crystals, *i.e.* periodic variations of the magnetic properties,[2–4] are discussed. Measurements have been carried out at the MAXYMUS end station at BESSY II. The photon energy has been tuned to the maximum of the Fe L_3 absorption edge to achieve maximum XMCD contrast. Signal detection and data analysis were carried out as described above.

3.1 Spin Waves in Antidot Lattices

Antidot lattices, *i.e.* periodic arrangements of holes called antidots, are a simple way to achieve a periodic modulation of magnetic properties and realize a magnonic crystal.[3,4,13] Here, we use an antidot lattice with 450 nm holes on a 900 nm square grid in a 50 nm Py film, which is sketched in Fig. 4a. The spin wave distribution in this sample under excitation at 3 GHz CW RF at an applied field of 30 mT is shown in Fig. 4b. Propagation of spin waves away from the excitation source (strip line, center) is clearly visible. Spin waves only propagate in the uninterrupted material channels between holes, which is intuitively expected. A slight self focussing within these channels is observed, as has been described by others.[14,15] This has been explained either by a slight frequency

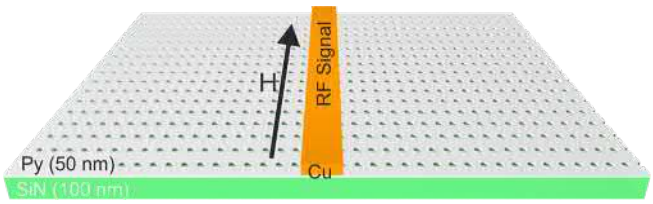

(a) Sketch of the antidot lattice sample: a 50 nm Py film is patterned with 450 nm holes on a square 900 nm grid.

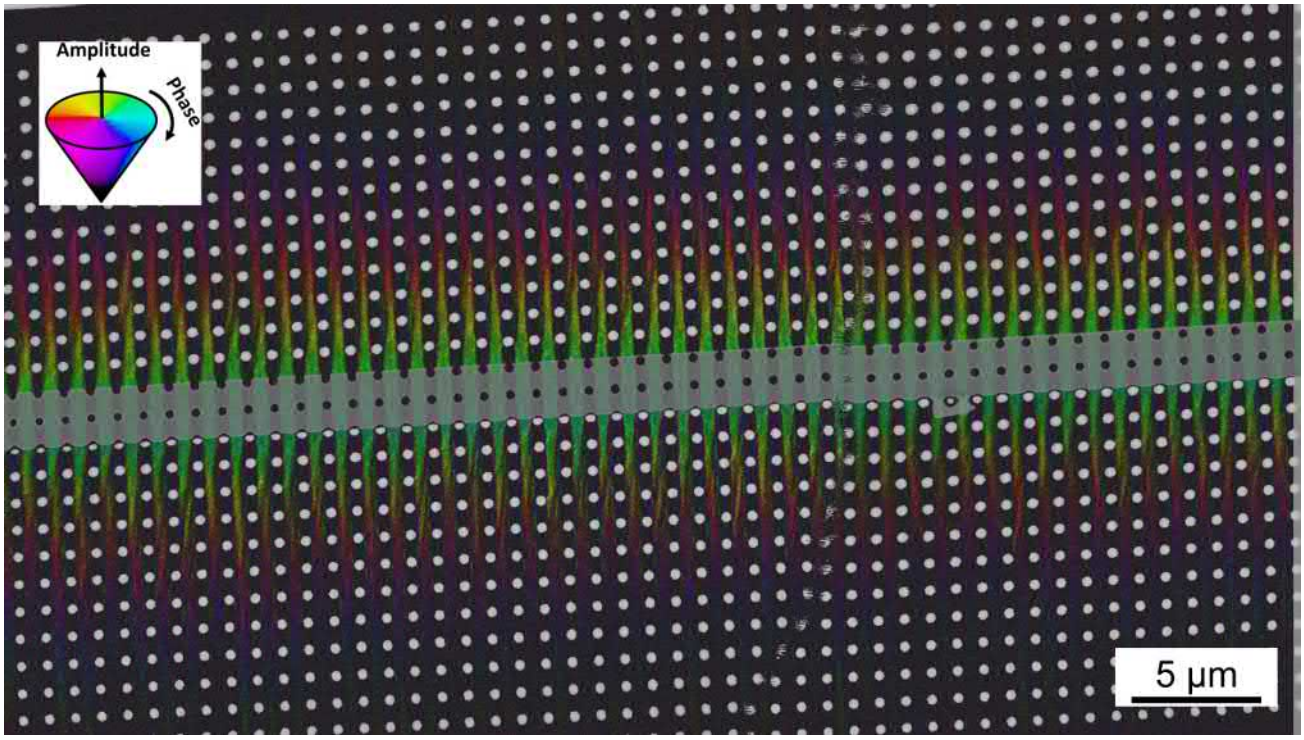

(b) Spin wave distribution in an antidot lattice at 30 mT applied field and with 3 GHz CW RF excitation. For a video animation see Video 1 at http://dx.doi.org/10.1117/12.2530326.1

Figure 4: Spin waves in antidot latices.

shift due to demagnetization effects at the hole edges[14] or an anisotropic isofrequency contour.[15] Furthermore, some spin wave intensity is diffusely scattered into the interstitial region between holes, which leads to gradual reduction of the spin wave amplitude.

Due to the ultimate resolution of STXM, additional features of the spin wave pattern are visible. Slight bowing of the spin waves at the hole edges, due to the local variation of the magnetization landscape, can be observed. Furthermore, some spin wave intensity propagates diagonally and is reflected back into the magnetic material channel at the hole edges. These features would remain elusive in techniques with lower resolving power. It is noteworthy that the measurement depicted in Fig. 4b has full HD resolution, *i.e.* 1920×1080 pixels, and was acquired in 5 hours, demonstrating the acquisition speed of time resolved STXM while maintaining zone plate limited resolution.

3.2 Spin Waves in Quasicrystals

Magnonic crystals have been widely investigated as they allow tailoring of the magnonic band structure and formation of forbidden bands in the spin wave spectrum.[4,6,16] This property can even be enhanced by turning to aperiodic structures like quasicrystals.[6,7,17,18] Here, we discuss a one-dimensional magnonic quasicrystal,

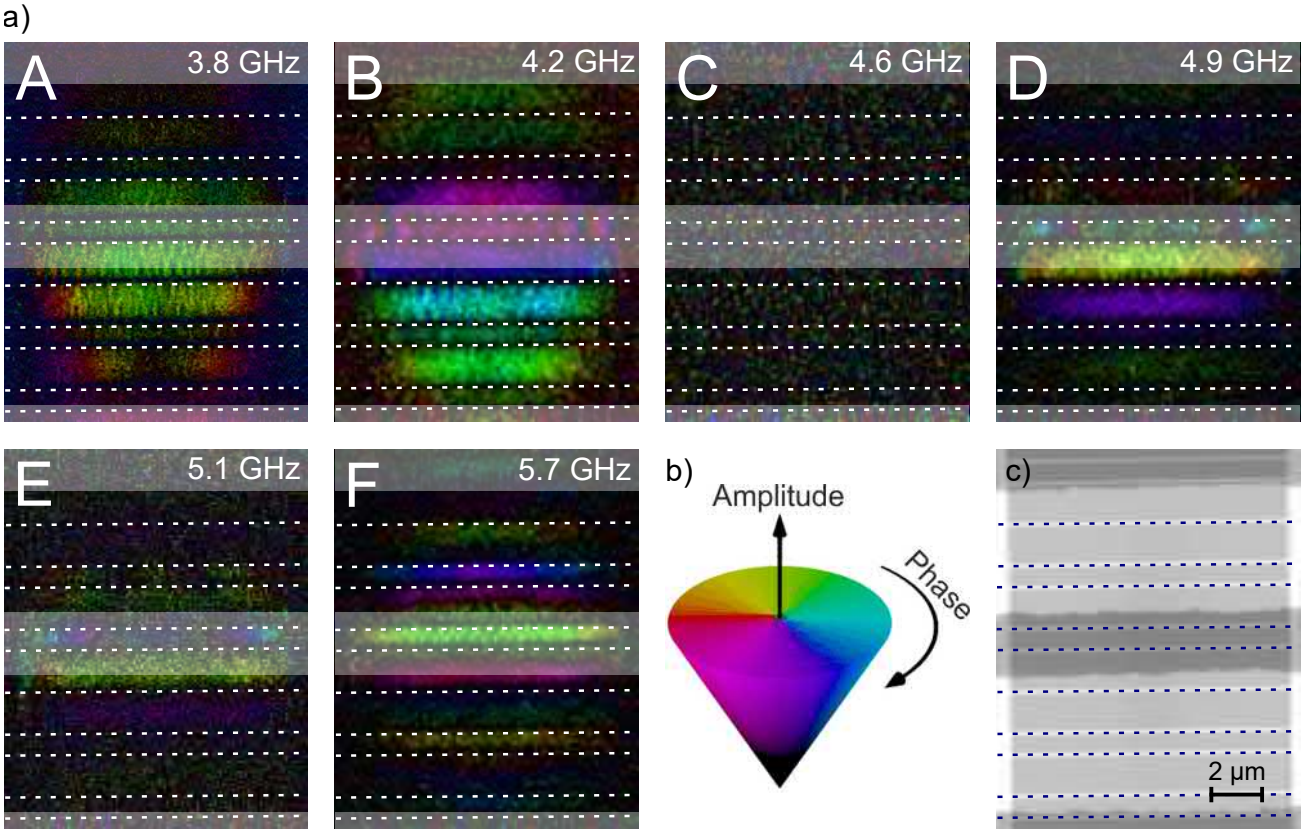

Figure 5: *(a)* SW amplitude and phase for different excitation frequencies at 5 mT. The transparent gray rectangles mark the position of the CPW and the dashed white lines mark the gaps between the stripes. *(b)* Color code for SW amplitude (brightness) and phase (color). *(c)* Static image of the Fibonacci structure (light gray) with the signal line (dark gray) near the center of the image, and the ground lines at the top and bottom edges of the image (dark gray). For a video animation see Video 2A-F at http://dx.doi.org/10.1117/12.2530326.2 Reproduced from.[6]

constituted by narrow (700 nm) and wide (1400 nm) Py stripes (thickness 30 nm) arranged according to the Fibonacci inflation rule. Time-resolved STXM measurements under CW excitation and an applied field of 5 mT are shown in Fig. 5. It is visible that spin waves can propagate in the quasicrystal, albeit its imperfect order (*cf.* Fig. 5 modes A, B, D and F at 3.8 GHz, 4.2 GHz, 4.9 GHz and 5.7 GHz, respectively). The gradual variation of phase is a clear indication of the propagating character of these spin wave modes.[6] Mode C in Fig. 5 at 4.6 GHz falls into a mini band gap that is specific to the quasicrystal where no spin wave excitation is allowed or observed,[6] while mode E at 5.1 GHz is in a regular band gap that would also be observed for a comparable regular magnonic crystal.[6] Here, STXM provides invaluable insights into these systems as it provides both a real-space and real-time access to spin wave data, that allows to immediately characterize spin wave modes at the nanoscale.

4. SUMMARY

We have discussed the methodical details of time-resolved STXM at the MAXYMUS endstation at BESSY II. A double lock-in scheme is used to detect single photon events. A first lock-in stage is implemented by a fast APD detector that is only active at the expected arrival time of photons. A second lock-in stage is realized by discriminating the single photon events with respect to an RF excitation source. This data is subsequently processed by a temporal and spatial FFT to yield amplitude, phase, and k-vectors of all spin waves excited in the

system. Furthermore, sophisticated RF excitations schemes can be realized by using an AWG with synchronized sampling rate, *e.g.* to simultaneously excite all allowed modes by a sinc pulse.

In the second part of the paper we have discussed to examples of magnonic crystals. In a regular magnonic crystal based on a quadratic hole array, we have shown the capability of maintaining zone plane limited resolution ($< 20\,\mathrm{nm}$) while scanning a large area (> 2 MPixel). The full fidelity of of spin wave modes propagating, reflecting, and scattering in the antidot lattices is recovered in the STXM movie. Furthermore, a magnonic quasicrystal was discussed, leveraging the STXM capability of simultaneous real-space and real-time measurement on the nanoscale. Thus, it was shown that spin waves can propagate in quasicrystals, albeit their disorder.

In conclusion, we have shown that STXM can be a valuable extension of the toolbox for magnonic research when ultimate resolution is required.

APPENDIX A. MULTIMEDIA FIGURES - VIDEO AND AUDIO FILES

Table 1: Information on video and audio files that must accompany a manuscript submission.

Item	File name	File size
Video 1	Video1.mp4 (should be mpeg mov or wmv)	658 KB
Video 2A	Video2A.mp4 (should be mpeg mov or wmv)	627 KB
Video 2B	Video2B.mp4 (should be mpeg mov or wmv)	610 KB
Video 2C	Video2C.mp4 (should be mpeg mov or wmv)	582 KB
Video 2D	Video2D.mp4 (should be mpeg mov or wmv)	610 KB
Video 2E	Video2E.mp4 (should be mpeg mov or wmv)	589 KB
Video 2F	Video2F.mp4 (should be mpeg mov or wmv)	566 KB

ACKNOWLEDGMENTS

The authors thankfully acknowledge Bernd Ludescher, Piotr Kuswik and Hubert Glowinski for thin film deposition and Michael Bechtel, Matthias Werner and Iuliia Bykova for support during beam times. We thank HZB for allocation of synchrotron radiation beamtime at the MAXYMUS end station. Financial support by the Baden-Württemberg Stiftung within the Kompetenznetz Funktionelle Nanostrukturen is gratefully acknowledged. The study has received funding from the European Union's Horizon 2020 research and innovation programme under the Marie Skłodowska-Curie GA No644348 (MagIC) and NCN Poland UMO-2012/07/E/ST3/00538. J.W.K. would like to acknowledge the support of the Foundation of Alfried Krupp Kolleg Greifswald and the National Science Centre of Poland Grant No.: UMO-2016/21/B/ST3/00452. J.R. would like to acknowledge the financial support from the Adam Mickiewicz University Foundation and from the National Science Centre of Poland under ETIUDA grant number UMO-2017/24/T/ST3/00173.

REFERENCES

[1] Kruglyak, V. V. and Hicken, R. J., "Magnonics: Experiment to prove the concept," *Journal of Magnetism and Magnetic Materials* **306**(2), 191–194 (2006).

[2] Kruglyak, V. V., Demokritov, S. O., and Grundler, D., "Magnonics," *Journal of Physics D: Applied Physics* **43**(26), 264001 (2010).

[3] Lenk, B., Ulrichs, H., Garbs, F., and Munzenberg, M., "The building blocks of magnonics," *Physics Reports* **507**(4-5), 107–136 (2011).

[4] Krawczyk, M. and Grundler, D., "Review and prospects of magnonic crystals and devices with reprogrammable band structure," *Journal of Physics: Condensed Matter* **26**(12), 123202 (2014).

[5] Groß, F., Träger, N., Förster, J., Weigand, M., Schütz, G., and Gräfe, J., "Nanoscale detection of spin wave deflection angles in permalloy," *Applied Physics Letters* **114**(1), 012406 (2019).

[6] Lisiecki, F., Rychły, J., Kuświk, P., Głowiński, H., Kłos, J. W., Groß, F., Träger, N., Bykova, I., Weigand, M., Zelent, M., Goering, E. J., Schütz, G., Krawczyk, M., Stobiecki, F., Dubowik, J., and Gräfe, J., "Magnons in a quasicrystal: Propagation, extinction, and localization of spin waves in fibonacci structures," *Physical Review Applied* **11**(5), 054061 (2019).

[7] Lisiecki, F., Rychły, J., Kuświk, P., Głowiński, H., Kłos, J. W., Groß, F., Bykova, I., Weigand, M., Zelent, M., Goering, E. J., Schütz, G., Gubbiotti, G., Krawczyk, M., Stobiecki, F., Dubowik, J., and Gräfe, J., "Reprogrammability and scalability of magnonic fibonacci quasicrystals," *Physical Review Applied* **11**(5), 054003 (2019).

[8] Hitchcock, A. P., "Soft x-ray spectromicroscopy and ptychography," *Journal of Electron Spectroscopy and Related Phenomena* **200**, 49–63 (2015).

[9] Nolle, D., Weigand, M., Schütz, G., and Goering, E., "High contrast magnetic and nonmagnetic sample current microscopy for bulk and transparent samples using soft x-rays," *Microscopy and Microanalysis* **17**(05), 834–842 (2011).

[10] Schütz, G., Wagner, W., Wilhelm, W., Kienle, P., Zeller, R., Frahm, R., and Materlik, G., "Absorption of circularly polarized x rays in iron," *Physical Review Letters* **58**(7), 737–740 (1987).

[11] Weigand, M., *Realization of a new magnetic scanning X-ray microscope and investigation of Landau structures under pulsed field excitation*, phd thesis (2014).

[12] Bonetti, S., Kukreja, R., Chen, Z., Spoddig, D., Ollefs, K., Schöppner, C., Meckenstock, R., Ney, A., Pinto, J., Houanche, R., Frisch, J., Stöhr, J., Dürr, H. A., and Ohldag, H., "Microwave soft x-ray microscopy for nanoscale magnetization dynamics in the 5–10 ghz frequency range," *Review of Scientific Instruments* **86**(9), 093703 (2015).

[13] Neusser, S. and Grundler, D., "Magnonics: Spin waves on the nanoscale," *Advanced Materials* **21**(28), 2927–2932 (2009).

[14] Demidov, V. E., Demokritov, S. O., Rott, K., Krzysteczko, P., and Reiss, G., "Self-focusing of spin waves in permalloy microstripes," *Applied Physics Letters* **91**(25), 252504 (2007).

[15] Kłos, J. W., Gruszecki, P., Serebryannikov, A. E., and Krawczyk, M., "All-angle collimation for spin waves," *IEEE Magnetics Letters* **6**, 1–4 (2015).

[16] Stamps, R. L., Breitkreutz, S., Åkerman, J., Chumak, A. V., Otani, Y., Bauer, G. E. W., Thiele, J.-U., Bowen, M., Majetich, S. A., Kläui, M., Prejbeanu, I. L., Dieny, B., Dempsey, N. M., and Hillebrands, B., "The 2014 magnetism roadmap," *Journal of Physics D: Applied Physics* **47**(33), 333001 (2014).

[17] Coelho, I. P., Vasconcelos, M. S., and Bezerra, C. G., "Transmission fingerprints in quasiperiodic magnonic multilayers," *Journal of Magnetism and Magnetic Materials* **323**(23), 3162–3167 (2011).

[18] Costa, C. H. O., Vasconcelos, M. S., and Albuquerque, E. L., "Partial band gaps in magnonic crystals," *Journal of Applied Physics* **109**(7), 07D319 (2011).